ICARUS 111 503–513 (1994)

Mirages and the Nature of Pluto's Atmosphere

J. A. STANSBERRY,[1] J. I. LUNINE, W. B. HUBBARD, R. V. YELLE, AND D. M. HUNTEN

Department of Planetary Sciences, Lunar and Planetary Laboratory, University of Arizona, Tucson, Arizona 85721
E-mail: Stansber@humbabe.arc.nasa.gov

Received May 16, 1994, revised July 14, 1994

We present model occultation lightcurves demonstrating that a strong thermal inversion layer at the base of Pluto's stratosphere can reproduce the minimum flux measured by the Kuiper Airborne Observatory (KAO) during the 1988 occultation of a star by Pluto. The inversion layer also forms the occultation equivalent of a mirage at a radius of 1198 km, which is capable of hiding tropospheres of significant depth. Pluto's surface lies below 1198 km, its radius depending on the depth of the troposphere. We begin by computing plausible temperature structures for Pluto's lower atmosphere, constrained by a calculation of the temperature of the atmosphere near the surface. We then trace rays from the occulted star through the model atmosphere, computing the resultant bending of the ray. Model light curves are obtained by summing the contribution of individual rays within the shadow of Pluto on Earth. We find that we can reproduce the KAO lightcurve using model atmospheres with a temperature inversion and no haze. We have explored models with tropospheres as deep as 40 km (implying a Pluto radius of 1158 km) that reproduce the suite of occultation data. Deeper tropospheres can be fitted to the data, but the mutual event radius of 1150 km probably provides a lower bound. If Pluto has a shallow or nonexistent troposphere, its density is consistent with formation in the solar nebula with modest water loss due to impact ejection. If the troposphere is relatively deep, implying a smaller radius and larger density, signficant amounts of water loss are required.

INTRODUCTION

Our knowledge of Pluto and its atmosphere has increased dramatically in recent years because of a series of mutual events in which Pluto and its moon Charon successively eclipsed each other, an occultation of a bright star by Pluto in 1988, and the advent of sensitive infrared and submillimeter spectrometric and photometric capabilities. In the present paper we utilize these diverse data sets together with new modeling to assemble a picture of the physical state of Pluto's surface and atmosphere, as well as to infer Pluto's density and bulk composition.

The stellar occultation of 1988, observed from the Kuiper Airborne Observatory (KAO) and other stations (Elliot *et al.* 1989, Millis *et al.* 1994), yielded peculiar lightcurves which have been interpreted in terms of haze extinction (Elliot and Young 1992) or a temperature inversion from the cold surface to a warm middle atmosphere (Eshleman 1989, Hubbard *et al.* 1990). The inversion model leads to the prediction of an atmosphere dominated by a mass 28 (e.g. N_2 or CO) molecule, rather than CH_4 (mass 16) (Yelle and Lunine 1989).

This prediction is strongly supported by the near-IR spectroscopy of Owen *et al.* (1993), which has detected the solid N_2 2.16-μm absorption band on Pluto. N_2 ice is a very weak absorber of near infrared light compared to CH_4, and it must dominate the surface in order to have been detected at all. N_2 also has a vapor pressure approximately 10^4 times larger than that of CH_4, the next most abundant molecule detected on Pluto's surface (Owen *et al.* 1993). Thus, N_2 is very likely the primary constituent of the atmosphere. Yelle and Lunine (1989) noted that the temperature of a pure N_2 atmosphere would be close to the surface temperature, giving a scale height of $\approx$30 km, but the presence of CH_4 at a mixing ratio of 10^{-3} (an overabundance of an order of magnitude compared to vapor pressure equilibrium if the CH_4 and N_2 ices are at the same temperature) would absorb enough solar infrared radiation to heat the atmosphere to more than 100 K. The 1988 occultation data (Elliot *et al.* 1989, Hubbard *et al.* 1990) revealed that the atmosphere had a scale height of approximately 60 km at a radius of about 1250 km, consistent with a N_2 atmosphere at 106 K (Millis *et al.* 1994). The overabundance of CH_4 necessary to achieve this agreement is paradoxical, because N_2 has replaced CH_4 as the primary atmospheric constituent, yet CH_4 is crucial for achieving atmospheric temperatures of 106 K. The presence effort goes a significant way toward resolving this paradox.

The inversion model has been criticized by Millis *et al.*

[1] Current address: NASA Ames Research Center mail stop 245-3, Moffett Field, CA 94035.

0019-1035/94 $6.00

(1994) and Stern (1992) on the grounds that it fails to achieve the very low stellar intensity observed by the KAO at lightcurve minimum, estimated to be ≤2% (J. Elliot, personal communication). We show that pure inversion models, with sufficiently large temperature gradients and no haze, can reproduce the low flux level observed at the bottom of the KAO lightcurve.

Regardless of whether the haze or thermal inversion layer model is used, the radius of Pluto inferred from the occultation data by Millis *et al.* (1994), <1180 km or ≈1195 km, is significantly larger than the radius inferred from the mutual event data (Buie *et al.* 1992). We explore the possibility that a troposphere, lying below the temperature inversion, would have escaped detection in the 1988 occultation data and hence could account for the discrepancy. We consider a range of troposphere depths (0 to 40 km), using previous work by Yelle *et al.* (1991) and Stansberry *et al.* (1992) on the temperature structure of Triton's troposphere as a model for Pluto's. We can reproduce the occultation data for any of these troposphere depths by varying the tropospheric temperature structure, so Pluto radii in the range 1158 to 1198 km are compatible with the occultation data. It should be noted that 1158 km is simply the smallest radius for Pluto that we have considered in detail: fits to the data can also be achieved for deeper tropospheres (smaller radii). The 1150 km mutual event radius of Buie *et al.* (1992) probably provides a lower bound on the real radius because models of the mutual event data by Young and Binzel (1993) that include the effect of limb darkening yield larger radii. Thus, we have covered the reasonably acceptable range of Pluto radii with these models. Finally, we show that these radii imply that Pluto's bulk density is between 1.78 and 2.01 g cm^{-3} and use current understanding of early solar nebula composition to discuss probable scenarios for Pluto's genesis and early evolution.

ATMOSPHERE MODELS

In this section we use albedo maps of Pluto's surface, constructed from 5 years of mutual event data (Buie *et al.* 1992, Young and Binzel 1994), to compute the distribution of surface temperatures on Pluto. By considering energy exchange between surface and atmosphere we then constrain the temperature of the atmosphere above the planetary boundary layer. This in turn is used as a boundary condition for models of the atmospheric temperature profile, the construction of which, and fitting to KAO lightcurve data, are described in the latter part of this section.

Surface–Atmosphere Energy Balance

In order to determine the temperature of Pluto's near surface atmosphere, we need to calculate the flow of energy between the surface and atmosphere. We approach this problem using the model of Stansberry *et al.* (1992), which was previously applied to energy balance between Triton's surface and atmosphere. The model calculates the partitioning of absorbed solar energy between radiation in the infrared, transport of latent heat *via* the sublimation and condensation of the volatile N_2 ices on the surface, and heating of the atmosphere by convection from warm regions on the surface. Conduction of heat into the subsurface is neglected. Using the albedo maps of Buie *et al.* (1992) and Young and Binzel (1993) from the 5-year series of mutual events we calculate bolometric albedo distributions on Pluto.

The scattering behavior of the surface depends on the single-particle scattering phase function. We used Hapke theory (Hapke 1981) to calculate bolometric albedos from the Buie *et al.* albedo map based on both the Henyey–Greenstein phase function for Triton's surface (Stansberry *et al.* 1992) and a phase function of the form $P(g) = 1 + b\cos(g)$, where $b = 2.0$ is the value consistent with the assumptions made by Buie *et al.* (1992) in deriving their albedo map. We only calculated bolometric albedos for the albedo map of Young and Binzel (1993) using this second phase function.

The bolometric albedo is then used to calculate surface temperatures and the N_2 ice distribution. In Stansberry *et al.* (1992) the coverage of N_2 ice was influenced by both the temperature of the surface (areas with equilibrium temperatures below the chosen N_2 temperature were taken to be N_2-covered) and by choosing a minimum albedo for N_2-covered areas. For Pluto the N_2 distribution is only weakly influenced by setting an albedo criterion. Table I summarizes the results of our surface–atmosphere energy balance calculation for Pluto. Values based on both albedo distributions are shown, where applicable.

TABLE I

	Buie *et al.*	Young and Binzel
N_2 ice temperature (assumed)	35.5 to 39.8 K	35.5 to 39.8 K
N_2 ice emissivity	0.5 to 1	0.5 to 1
Atmospheric temperature	53 K	51 K
Temperature of areas heating the atmosphere	54 K	52 K
Typical upward heat flux	5.5 erg cm^{-2} sec^{-1}	9 erg cm^{-2} sec^{-1}
Downward heat flux in		
N_2 free areas	0.1 erg cm^{-2} sec^{-1}	0.1 erg cm^{-2} sec^{-1}
N_2 covered areas	0.3 erg cm^{-2} sec^{-1}	0.3 erg cm^{-2} sec^{-1}

Average values are given for the temperatures of areas free of N_2 ice and the heat fluxes associated with them.

The maximum surface temperatures (50 to 55 K) are considerably higher than the warmest temperatures calculated for Triton by Stansberry *et al.* (1992), namely 45 K. This is because the ice-free regions on Pluto are at the subsolar point, whereas on Triton the subsolar point is dominated by N_2 ice at this season. Also, the albedo contrast between N_2-covered and N_2-free regions on Pluto is much larger than on Triton. As a result, the temperature of Pluto's atmosphere near the surface is about 10 K warmer than Triton's.

The model produces a globally averaged atmospheric temperature at the top of the planetary boundary layer. The assumption of a single temperature for the atmosphere at that level results in an overestimate of the convected heat flux between the surface and atmosphere. Negligible errors in surface temperature are introduced by this simplification because these heat fluxes are small compared to the solar heat flux. In reality, the temperature of the atmosphere over warm areas will be higher than over colder areas. This gradient in atmospheric temperature may drive a circulation, producing a region of negative temperature gradient, i.e., a troposphere. Radiation and conduction are neglected within the lower atmosphere, a simplification that is justified *post facto* by the observation that the upward convected heat fluxes we calculate exceed the conducted stratospheric heat flux by over two orders of magnitude.

Troposphere

Rather than develop a detailed model of a hypothetical Pluto troposphere, we have considered a variety of plausible schematic troposphere structures. The most basic measure of the troposphere is its depth, which we have allowed to vary from 0 to 40 km. The temperature gradient in the troposphere is a more complicated issue. Characteristic temperature gradients associated with convective tropospheres are the wet pseudoadiabat, -0.1 K km^{-1}, or the dry adiabat, -0.75 K km^{-1}, above the planetary boundary layer. While an upward convected heat flux produces negative temperature gradients, downward convected heat fluxes increase the temperature gradient and can result in positive temperature gradients if the downward heat flux is more than ≈ 0.5 erg cm^{-2} sec^{-1} (Stansberry *et al.* 1992). We have explored a range of models for Pluto's troposphere incorporating lapse rates appropriate to both upward and downward convection, either singly or in combination (two different lapse rates applying over two layers in the troposphere), with a mix of wet and dry lapse rates.

Upper Atmosphere

We use a "Bates model" to describe the temperature profile of the atmosphere above the tropopause (Bates 1951). We note that the Bates model is a mathematical convenience rather than either an empirical or first principles model of the expected temperature profile. Thus, our model atmospheres should be taken as only semiquantitative descriptions of Pluto's atmosphere rather than as rigorous constraints on the exact details of the atmospheric parameters. The temperature profile is specified by

$$T(z) = T_\infty [1 - ae^{-\tau\zeta}], \tag{1}$$

where

$$a = 1 - \frac{T_0}{T_\infty} \tag{2}$$

and

$$\tau = \frac{(dT/dz)_0}{T_\infty - T_0}. \tag{3}$$

The subscripts ∞ and 0 refer to values at large altitudes and at the tropopause. We use $T_\infty = 106$ K and $T_0 = 50$ K. The value of $(dT/dz)_0$ is adjusted to fit the knee in the KAO lightcurve. ζ, the geopotential height, is a gravity-scaled height coordinate defined by

$$\zeta = \int_{z_0}^{z} \frac{g(z)}{g_0} dz. \tag{4}$$

Determination of Upper Atmospheric Structure by Fitting the KAO Lightcurve

We use three critical points in the KAO lightcurve to determine the atmospheric structure above the tropopause. These three points, taken from Elliot and Young (1992), are the time to half light, $t_{\frac{1}{2}}$, time to the "knee" (see Fig. 3) in the lightcurve, t_k, and the time for the flux to fall to $1/e$ of the value at the knee, t_τ. We derive a reference pressure at 1250 km (determined by $t_{\frac{1}{2}}$) of 1.13 μb. The spacing between $t_{\frac{1}{2}}$ and t_τ determines the surface radius or tropopause level, depending on the model being considered, which we find to be 1198 km. Finally, the interval between t_τ and t_k constrains the value of the temperature gradient, $(dT/dz)_0$, at the base of the stratosphere. We find that we require $(dT/dz)_0 \approx 30$ K/km to fit the knee in the lightcurve. This temperature gradient is largely an artifact of our choice of the Bates model, because the knee is actually formed by the portion of the atmosphere where the temperature profile is strongly curved, around 1210 km. The large temperature gradient we find in these

models is required to provide enough curvature at those levels, and does not relate directly to the shape of the knee.

We present our models in terms of the radius from the center of Pluto's shadow on Earth rather than times, and the corresponding values of these radii are $r_i' = 1174.61 \pm 2.12$ km, $r_k' = 1124.68 \pm 2.25$ km, and $r_\tau' = 1091.26 \pm 3.15$ km. Our fits reproduce the location of these features to within 0.5 km. Number density is derived from hydrostatic equilibrium and the constraint that the pressure (assuming an N_2 composition) at 1250 km is 1.13 μb.

Figure 1 illustrates a subset of the temperature profiles we have explored, and Table II summarizes some derived atmospheric parameters. Elliot and Young (1992) found a reference pressure of 1.26 ± 0.35 μb at 1250 km, somewhat larger than the value we derive, 1.13 μb. The Pluto radii derived from their temperature inversion models and those of Millis *et al.* (1994), ≈1195 km, are very slightly smaller than the zero-thickness troposphere radius in our models, 1198 km. The source of these minor discrepancies is unclear at present, but probably lies in the details of the assumed temperature profile.

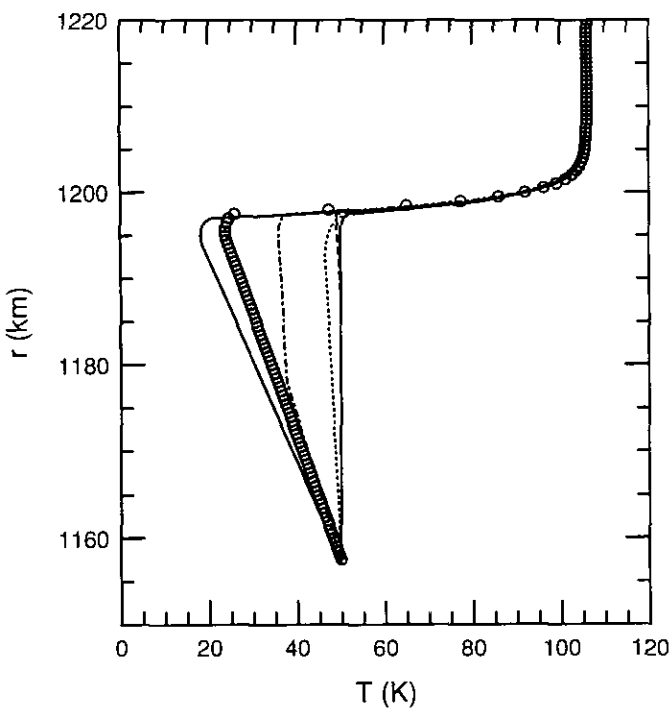

FIG. 1. Various temperature profile models used in the synthesis of lightcurves. All profiles are essentially identical above the tropopause at $r = 1198$ km. The "knee" in the KAO lightcurve is formed in the region near 1205–1210 km. Lightcurves shown in Figs. 3 and 4 correspond to a typical temperature profile (∘ ∘ ∘).

TABLE II

Reference radius	1250 km
Reference pressure	1.13 μb
Molecular mass	28
Temperature of stratosphere	106 K
Tropopause radius	1198 km

Depth of troposphere (km)	Surface pressure[a] (μb)	Equivalent N_2 temperature[b] (°K)
0	3.1 μb	35.2 (α)
5	3.4 μb	35.3 (α)
10	4.2 μb	35.6 (β)
20	6.8 μb	36.4 (β)
40	24 μb	38.4 (β)

[a] Approximate—depends on our assumption of a Bates model stratosphere and $(dT/dz)_{trop} = 0.7$ K km^{-1}.
[b] Assuming vapor pressure equilibrium.

SYNTHESIS OF LIGHTCURVES

Theory

In this section we describe the synthesis of lightcurves, with the aim of constraining the depth of a possible troposphere and hence the minimum radius of the solid planet. We start with a spherically symmetric model atmosphere in which the molecular number density, n, is known as a function of radius, r. The optical axis of the occultation lies on a line passing through the occulted star and the center of Pluto. The observer is located at a distance D from Pluto and a distance r' from the optical axis, with $D \gg r'$. Because Pluto is unresolved in the occultation observations, the multiple signals are summed into a single value for the total flux from the occulted star, $\phi(r')$, normalized such that $\phi = 1$ for the unocculted star.

The value of ϕ is calculated, for a given value of r', by summing over all stationary phase paths from the star to the observer and by calculating the amplification or deamplification of the flux for each path by determining the curvature of the wavefront imposed by the atmosphere. In this model there is no net loss of photons above the tropopause by scattering or absorption. The effect of tropospheric clouds has been included in some models for stationary phase paths which pass through the troposphere. Each point r' is linked by stationary phase paths to at least two corresponding closest-approach radii r in Pluto's atmosphere, located on opposite sides of the optical axis. For a given stationary phase path, refraction within the troposphere can give rise to a singular point where dr'/dr vanishes and the ray-optical flux ϕ becomes infinite (although the average stellar flux over a small finite time interval remains finite). These points divide, on the r' axis, regions where the corresponding number of

stationary phase paths double (e.g., from two to four) and are therefore caustics. In such cases an observer with infinite resolution would see multiple mirage-like images of the occulted star located at different values of r in Pluto's atmosphere, e.g., one image on the observer's side of the optical axis and three images on the opposite side.

We convert a theoretical lightcurve to a lightcurve which can be directly compared with observations as follows: (1) At each value of r', the flux from multiple stellar images is summed to give a single value of ϕ. (2) We compute a series of r' values corresponding to equally spaced intervals in time t, using the formula $r' = \sqrt{r'^2_{\min} + v^2(t - t_{\min})^2}$. Each observing station has a speed v with respect to the shadow plane, an impact parameter $r'_{\min}$ with respect to the center of the shadow, and a time $t_{\min}$ at which it reaches $r'_{\min}$. (3) We perform a triangular convolution of the model flux over a stellar profile with "radius" r_* (typically, $r_* \approx 1.6$ km). (4) Finally, noise is added to the synthesized lightcurve at the level quoted in Millis *et al.* (1994) for the station under consideration. Synthesis of noise plays a critical role in this discussion: we shall argue that possible tropospheric caustics are unobservable owing to the low S/N values for Pluto occultation lightcurves from the most central chords. We consider two types of noise, instrumental shot noise and scintillation. Shot noise is simulated by adding random signal increments with Gaussian statistics to each synthetic lightcurve, choosing the rms amplitude of the increments to match the actual signal-to-noise ratio (S/N) for the station. The synthetic shot noise is taken to be independent of ϕ, as would be appropriate for a signal dominated by the background sky and Pluto signal and by dark current. Scintillation is produced by small-scale density fluctuations in Earth's atmosphere and in Pluto's occulting atmosphere. Scintillation in Earth's atmosphere mainly occurs at much higher frequencies than those sampled in the Pluto data sets and is negligible for our purposes. In the following section we discuss the effect of small-scale structures in Pluto's atmosphere on occultation lightcurves.

Constraints on Scintillation Amplitude from the Data

Data from the 1988 Pluto occultation observed with the KAO have the highest S/N of any data set, and can be used to place limits on scintillations produced by density fluctuations in Pluto's atmosphere. In principle scintillations might affect our inferences about the large scale structure of Pluto's atmosphere, so we have evaluated them in our models as follows. First, we assume that the density perturbations are only in the vertical direction so that the atmosphere remains radially symmetric. Second, we assume that the amplitude of the density fluctuations is proportional to the mean density and that they are a superposition of waves having a Kolmogorov wavenumber spectrum over a range of radial wavenumbers (Narayan and Hubbard 1988).

Only a few scintillations are seen in the KAO lightcurve, and even these may not be statistically significant; this is in marked contrast to a typical Neptune occultation lightcurve as analyzed by Narayan and Hubbard (1988). We find that a relative root-mean-square density fluctuation in Pluto's atmosphere >0.002 is required for detectable scintillations to appear, but that levels >0.003 give scintillations larger than seen in the KAO lightcurve. Such density fluctuations are about an order of magnitude smaller than those inferred for the stratosphere of Neptune. In general, synthesized Pluto scintillations appear with significant amplitude only above the "knee," and have only a slight effect on the positions of caustics. The synthetic lightcurves presented below include scintillations with an RMS amplitude of 0.003. The corresponding RMS temperature fluctuation is ≈ 0.2 K.

Effect on the Lightcurve of a Diurnal Boundary Layer

As shown in Fig. 1 of Millis *et al.* (1994), all of the tracks of observations of the 1988 Pluto occultation were nearly parallel to Pluto's rotation axis. The Charters Towers and KAO tracks largely sampled early morning portions of Pluto's atmosphere after a night lasting about 3 Earth days, while stations such as Auckland, Black Birch, Hobart, and Mt. John largely sampled atmosphere that had been in daylight. The bottom part of Pluto's atmosphere should share the diurnal variation of the surface temperature, as is observed on Mars and in desert areas of Earth. The amplitude of the diurnal temperature variation at the surface depends on the thermal inertia of surface layers, but is unlikely to exceed 5 K. The thermal skin depth is given by $h \sim \sqrt{\chi t}$, where χ, the eddy diffusion coefficient, is taken to be ~ 10 m^2 sec^{-1}, by analogy with earth's troposphere, and $t \sim 3 \times 10^5$ sec. This yields $h \sim 1$ km. With an amplitude of ≈ 5 K for the temperature variation assuming constancy of pressure, the relative variation in density and hence refractivity would be of order 0.1 over the interval h. The boundary layer shifts the amplitude and position of caustics in some models, but its influence is not as pronounced as some of the other effects considered. The boundary layer in some cases has a small effect on the minimum flux value that would have been observed by the KAO. We do not consider it further.

Effect of a Troposphere on the Lightcurve

Figure 2 displays model lightcurves corresponding to some of the atmosphere models in Fig. 1. The presence of a troposphere causes the appearance of caustics (spikes) in the observed flux, typically in the central region

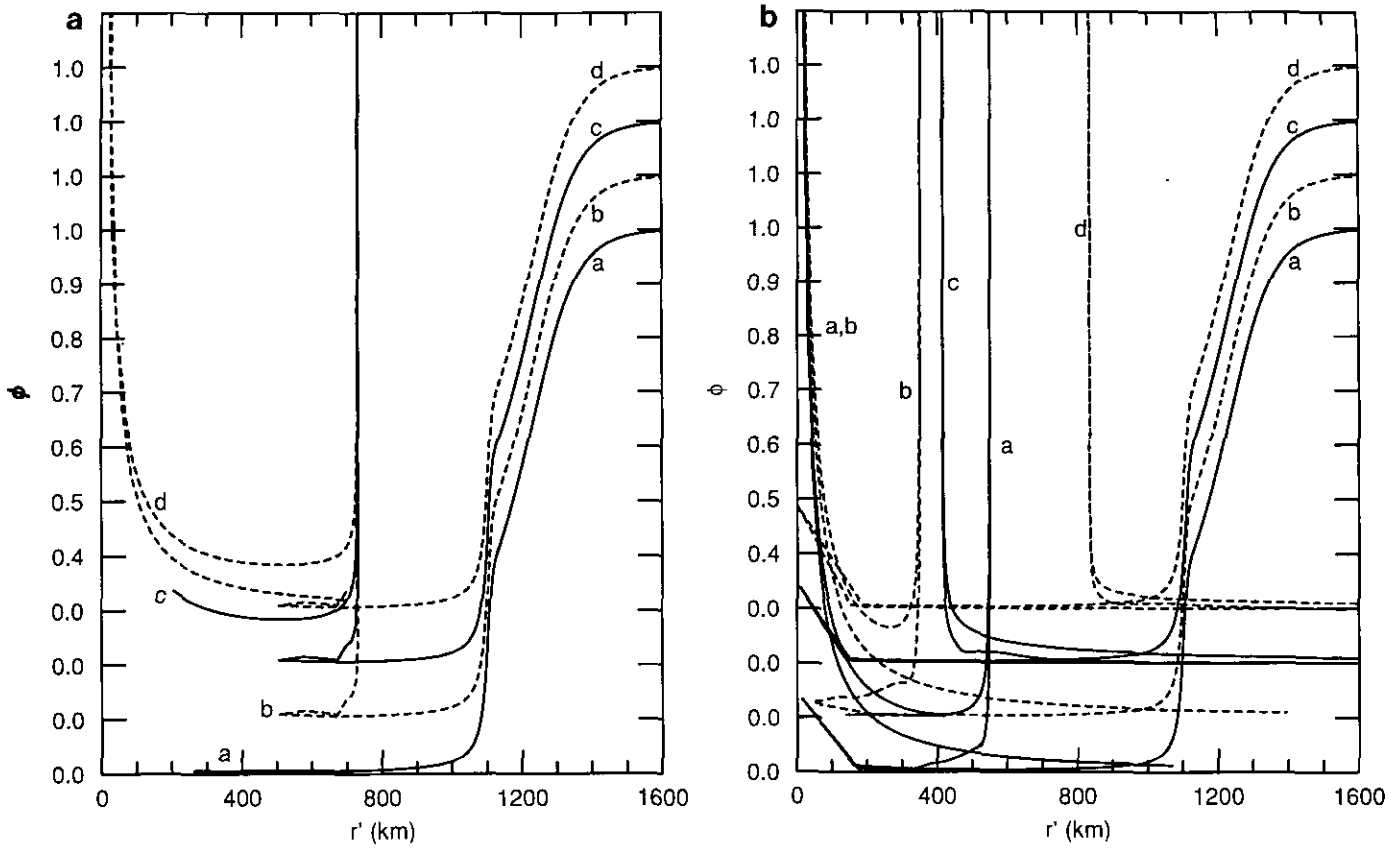

FIG. 2. (a) The effect on the lightcurve of adding tropospheres of various depths. The temperature gradient in the troposphere was set equal to 0 K km^{-1}, and curves a–d are for troposphere depths of 0, 5, 20, and 40 km, respectively. The lightcurves have been offset by 10% in normalized flux for clarity. (b) The effect of changing the tropospheric temperature gradient on the lightcurve. Curves a–d are for tropospheric temperature gradients of −0.2, −0.4, −0.65, and −0.75 K km^{-1}, respectively. The troposphere depth was 40 km.

of the shadow. Another important but more subtle effect is a slight increase in flux at the minimum in the lightcurve. The KAO measurements limited the minimum flux to less than about 2% (J. L. Elliot, personal communication). We find residual fluxes of somewhat less than 1% for the atmosphere without a troposphere, and of less than 2% for some cases with tropospheres. Below we describe atmosphere models which both meet the minimum flux requirement and which do not create caustics that would have been detected in any of the six lightcurves taken during the 1988 occultation. We note that the addition of a troposphere has no noticeable effect on the knee.

Figures 2a and 2b illustrate the effect of changing the tropospheric depth and temperature gradient, respectively. The curves from bottom to top are for increasingly deeper tropospheres (Fig. 2a) or for tropospheres with increasingly negative temperature gradients (Fig. 2b). The lightcurves are multivalued in this representation for reasons described earlier. In Fig. 2a the image of the star strikes the surface at $r' = 260$ km in the absence of any troposphere, but with a troposphere, rays passing below the tropopause are refracted to larger values of r' and are focused into a caustic at about $r' = 730$ km. For the 5-km deep troposphere the caustic is truncated by Pluto's limb just as it begins to form. The deeper tropospheres allow the 730-km caustic to fully form before the star dives behind Pluto, and in the case of a 40-km troposphere a central caustic is produced and the stellar image begins a second trek outward in r' before the star is finally extinguished by Pluto. The excursions at very low flux levels between $r' = 500$ and 700 km are due to numerical noise in the model atmosphere.

Under our assumption, justified in previous sections, that the near surface atmospheric temperature is 50 K, different tropospheric temperature gradients produce different tropopause temperatures. Figure 2b shows that the positions of the caustics in the lightcurves are quite sensitive to the tropopause temperature. The importance of this effect can be seen by examining Fig. 2a, in which the tropopause temperature was 50 K in all cases, and the caustics all occur at the same position. By comparison, here the caustics occur at various locations which vary in a systematic way with the tropopause temperature, T_{trop}. As T_{trop} becomes lower, the position of the caustic

first moves toward the center of the shadow (curves a and b), reaching it for a tropospheric temperature gradient of -0.5 K km^{-1}, and then moves back outward (curves c and d) as the temperature gradient approaches the dry adiabat. The observation of such caustics could in principle be diagnostic of the temperature at the tropopause and the depth of the troposphere. All of the caustics in this and Fig. 2a occur at r' values smaller than the minimum r' probed by the KAO (868 km, Millis *et al.* 1994) and would not be visible in that data set.

Deep tropospheres with any significant tropospheric temperature gradient might have been detected by the KAO in ways other than the position and strength of their caustics. In those lightcurves (Fig. 2b) significant flux is contributed to the region $868 < r' < 1000$ km by rays passing through the atmosphere on the far limb of Pluto. The flux there is limited to <2% by the KAO data (J. L. Elliot, personal communication). Clouds *in the troposphere* could mitigate this problem. A cloud layer 10 km thick, having the tropopause as its upper boundary, and vertical optical depth $\simeq 0.1$, such as were observed in Triton's troposphere by the Voyager 2 imaging system (Rages and Pollack 1992), would diminish the far limb tropospheric flux by one-third. As shown in Figs. 3 and 4, this brings our model lightcurves into agreement with the minimum light established by KAO. The clouds proposed here would not contribute to the formation of the knee in the KAO lightcurve, because they lie well below the level in the stratosphere where the knee is formed, between 1205–1210 km. The clouds proposed here should not be confused with the haze layer originally proposed by Elliot *et al.* (1989) as a possible cause of the knee.

The presence of a troposphere on Pluto certainly has the potential of producing easily observed effects in occultation lightcurves, but would these effects have been seen in the 1988 occultation data? Figure 3 shows model lightcurves calculated for the KAO occultation chord. Curve (a) is calculated for the model atmosphere denoted by ∘ ∘ ∘ in Fig. 1 (with a 40-km-thick troposphere having a temperature gradient of -0.7 K km^{-1}), with and without a tropospheric cloud layer (the model with a cloud layer has a lower minimum flux). In curve (b), which is offset downward for clarity, Pluto scintillations corresponding to a relative density fluctuation of 0.003 are added to the model with a cloud layer. Curve (c) shows the same model, but with shot noise added. Curve (d) shows the actual KAO data. The minimum flux in the model KAO lightcurve with no clouds is about 4%, but if we add a 10-km-thick cloud layer with a vertical optical depth of 0.13 and an opacity scale height of 10 km, the minimum flux drops to 2%.

A more telling station from the point of view of revealing the troposphere is Toowoomba, which has a closest approach distance $r_{min} = 188$ km (Millis *et al.* 1994). Figure 4 shows, in a manner analogous to that of Fig. 3, the synthetic lightcurves and actual data for this station. Although caustics are prominent in the noise-free theoretical curve, by the time this curve has been degraded to the noise level in the observation, they are indistinguishable from the noise in the data. Thus, the occultation data do not exclude the possibility that Pluto has a troposphere which is quite deep.

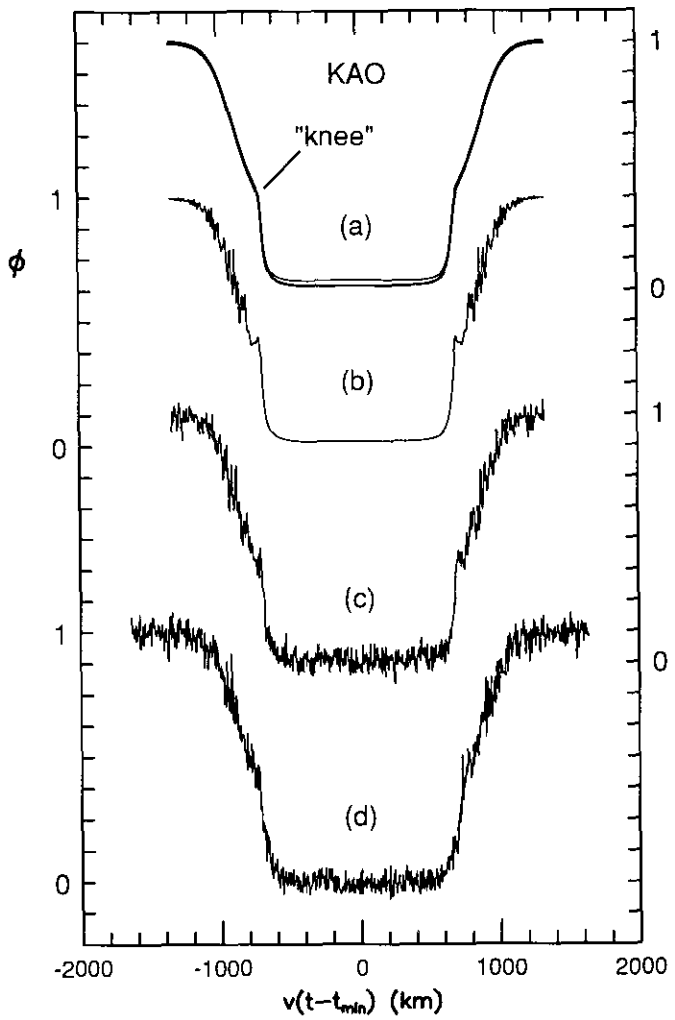

FIG. 3. Comparison of theoretical and measured lightcurves for KAO. (a) Theoretical lightcurve for temperature profile (∘ ∘ ∘) shown in Fig. 1, with and without a cloud layer. (b) Same as (a), with scintillations added. (c) Same as (b), with noise added. (d) KAO data.

IMPLICATIONS OF THE RADIUS FOR PLUTO'S DENSITY AND ORIGIN

The occultation analysis presented above provides constraints on Pluto's density and composition which have implications for the chemical reservoirs from which the Pluto/Charon system formed. The high atmospheric tem-

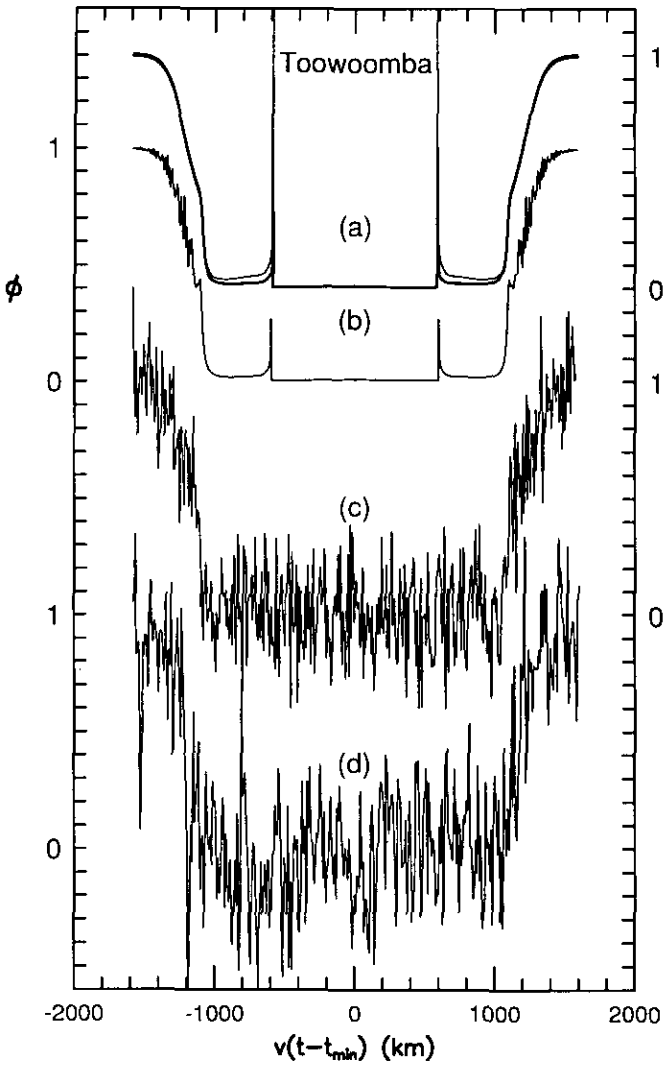

FIG. 4. Comparison of theory and data for Toowoomba. (a) Theoretical lightcurve for temperature profile (∘ ∘ ∘) shown in Fig. 1, with and without a haze layer. (b) Same as (a), with scintillations added. (c) Same as (b), with noise added. (d) Toowoomba data, kindly provided by L. Wasserman and R. Millis.

perature required to fit the occultation data, which confirms earlier analyses of Hubbard *et al.* (1991) and Millis *et al.* (1994), implies a predominance of gases of molecular weight close to 28 in addition to the CH_4 required for heating (Yelle and Lunine 1989). Based on solar elemental abundances and molecular stability, CO and N_2 are the best candidates. The most recent near-infrared spectroscopy of the surface of Pluto (Owen *et al.* 1993) reveals solid phases of nitrogen, methane, and carbon monoxide, in the ratio 100 : 1.5 : 0.5. Comparison of the ratio of the three volatiles reveals two issues of significance. First, the N_2-to-CO ratio is orders of magnitude larger than that expected in any primitive reservoir from which Pluto could have formed, including molecular cloud grains (Van Dishoeck *et al.* 1993) or material processed through the Sun's protoplanetary disk (hereafter "solar nebula") (Lewis and Prinn 1980). This suggests significant loss of carbon monoxide after formation and/or production of N_2 from an additional source, possibly ammonia which is relatively abundant in molecular cloud grains (Van Dishoeck *et al.* 1993). Second, the presence of significant amounts of CH_4 on Pluto weighs in favor of relatively unaltered molecular cloud material, for which the CH_4-to-CO ratio is not too dissimilar from that derived spectroscopically for Pluto's surface; gas processed in the solar nebula would be expected to have much smaller CH_4 abundances unless very efficient catalysis of CO reduction on grains were achieved (Engel *et al.* 1990). Grains from the molecular cloud core which went to form the Solar System could have fallen into the solar nebula with modest heating and processing (Lunine *et al.* 1991), avoiding significant chemical reequilibration provided radial mixing were inefficient in the solar nebula, as argued by Stevenson (1990) (but see Prinn 1990).

The density of Pluto can be used to infer the planet's bulk ratio of "rock" (i.e., silicates and metals) to "ice" (water and more volatile compounds) and hence something of its early history. If Pluto's radius is at the upper end of the range we calculate above, 1198 km, its astrometrically determined mass $1.31 \pm 0.024 \times 10^{25}$ g (Null *et al.* 1993), yields a bulk density for the planet of 1.82 g cm^{-3}. (A more recent mass determination by Young et al. (1994) yields $\rho = 1.78$.) If Pluto's radius is 1158 km, its density is 2.01 g cm^{-3}. The link between the bulk density and the rock-to-ice ratio of the planet comes through the fact that carbon is roughly half the abundance of oxygen in solar material, and CO will tie up oxygen preferentially relative to water. Hence the rock-to-ice ratio and bulk density of an icy body is determined by how much carbon was locked up in the primordial gas as CO (and secondarily CO_2, which under relevant conditions is less abundant than the monoxide). Complicating the issue is the abundance of carbon locked in involatile organic phases; it may represent half the carbon in interstellar clouds, and creates an additional uncertainty in using bulk density to infer bulk composition.

In Fig. 5 we plot the ice mass fraction versus bulk density of Pluto (solid line). The positions of the error bars at $\rho = 1.82$ and 2.01 g cm^{-3} reflects the range of Pluto densities we derive from our lightcurve modeling. The length of the error bars is based on a range of Pluto interior models which include the uncertainty due to differing degrees of hydration of the rock component (Simonelli and Reynolds 1989, McKinnon and Mueller 1988); they are extended to the lowermost tick marks to allow for the additional uncertainty due to the presence of organics. These ice mass fractions are compared with the theoreti-

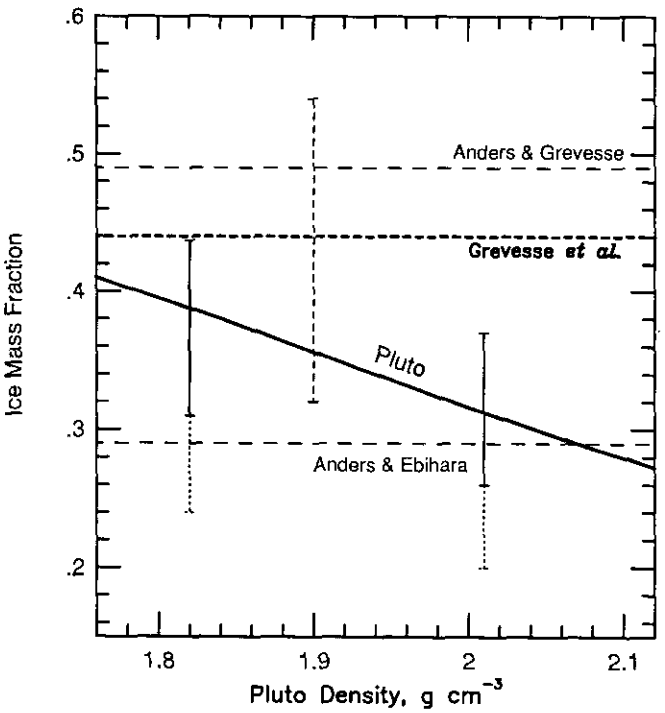

FIG. 5. Ice mass fraction versus density of Pluto. Solid line is Pluto, error bars show range corresponding to different models. Lowermost error bar in each case makes an additional allowance for the presence of organics, which would lower the ice mass fraction. Horizontal dashed lines are predictions from elemental abundance determinations; as described in text, the Grevesse values (with dashed error bar) are most up-to-date.

cal value computed as described in the previous paragraph, assuming that the predominant phase of carbon is CO (not CH_4), which soaks up a significant fraction of the oxygen that would otherwise mostly form water. Revised elemental abundances for the Sun are reflected in the three horizontal lines; the oldest being Anders and Ebihara (1982) and the most recent Grevesse *et al.* (1991). The dashed error bar reflects the uncertainty in the most recent determination. If involatile organic phases are present in the material, the horizontal lines should slide upward an amount dependent upon the composition and abundance of the organics. If half the carbon is in the form of organics which contain no oxygen (an extreme assumption), the Grevesse line should be moved up to roughly the top of its error bar.

The ice mass fraction we estimate for Pluto is systematically below the theoretical value based on the elemental abundance determination of Grevesse *et al.* (1991), although for the larger radius/lower density Pluto there is nominal agreement between the theoretical value and our estimate. An underabundance of ice is most readily explained by water loss during or after formation. Models for the formation of Charon by giant impact (McKinnon 1989) suggest some water loss, but loss of a significant fraction of the water (i.e., half) appears difficult. Moreover, Triton's density of 2.05 g cm^{-3} as determined from Voyager 2's trajectory (Tyler *et al.* 1989) implies a large amount of water loss; its dynamical history associated with capture by Neptune could conceivably lead to more water loss than from Pluto, though this has yet to be modeled in detail.

Most important is that Fig. 5 illustrates a cautionary note regarding cosmogonic interpretations of density: error bars on elemental abundance determinations and the range of possible interior models limit the strength of the conclusions which can be drawn. It is essential to decrease the uncertainty in the elemental abundance determinations, since constraints on the interior models are not likely to improve in the near future.

CONCLUSIONS

We fitted the KAO lightcurve using atmosphere models containing a troposphere and an inversion layer at the base of the stratosphere. The inversion model implies the presence of N_2 and/or CO in the atmosphere along with CH_4, and the recent spectroscopic detection of these species as solid phases on the surface is consistent provided that the CH_4 ice is a few degrees warmer than N_2/CO ices. The warm regions on Pluto's surface may explain the CH_4 mixing ratio of $>10^{-3}$ required in the Yelle and Lunine (1989) model for heating Pluto's upper atmosphere to $\approx$106 K. A mixing ratio of 10^{-3} is well above what is obtained if the CH_4 and N_2 ices are at the same temperature, but if CH_4 exists on the surface at temperatures a few Kelvin warmer than the N_2 ice, a mixing ratio of 10^{-3} is reasonable.

The existence of regions with distinctly different temperature may also resolve the conflict between the infrared and sub-millimeter surface temperatures of Pluto. Sykes *et al.* (1987) measured infrared brightness temperatures for Pluto of $\approx$58 K. Later microwave observations (Altenhoff *et al.* 1988, Stern *et al.* 1993) found microwave brightness temperatures of 35–40 K. Our lightcurve fits and hydrostatic equilibrium require Pluto's N_2 ice to be at 35.5 K if there is no troposphere, and 39.8 K for a 40-km troposphere, but we also find surface temperatures of $\approx$55 K in areas free of N_2. Such a two-temperature-component surface model appears to be confirmed by the submillimeter photometry of Jewitt (1994).

The model lightcurves reproduce the shape and location of the knee in the lightcurve as well as the minimum flux observed by the KAO. In some cases we require a relatively thin layer of clouds (normal optical depth $\approx$0.1) below the tropopause in order to meet the minimum flux constraint. Our model lightcurves also agree qualitatively with other measured lightcurves from the 1988 Pluto oc-

cultation, and we find that none of the data rules out the presence of a substantial (up to 40 km) troposphere. The model atmosphere we employ is not based on a physical model of processes in Pluto's atmosphere, nor is it derived directly from an inversion of lightcurve data. Because of this, the details of the temperature and pressure structure presented here are somewhat uncertain, and the best physical representation of the atmospheric structure is still that of Hubbard *et al.* (1990), which was based on an inversion of the KAO data.

Previous occultation determinations of Pluto's radius, for example the 1195 km of Millis *et al.* (1994) reflect only the bottom of the stratospheric temperature inversion. Our fits put the base of the inversion at 1198 km, with a possible mirage caused by an underlying troposphere, hence pushing the surface radius downward from 1198 km. If the troposphere is thin (< 10 km) Pluto's radius is near 1190 km, and, combined with compositional data, suggests that it formed from outer solar nebula material with relatively little water loss during and after formation. This fits with the nebular formation scenario for Triton, which would have started with a density close to Pluto's, but then became more dense *via* water loss during its capture by Neptune, reaching its current density of 2.05 g cm^{-3}. However, we show that 40-km-deep tropospheres, which would nearly reconcile the occultation and mutual event radius determinations for Pluto, are also possible. If the troposphere is 40 km deep, implying a radius of 1158 km, Pluto would have had to undergo considerable loss of primordial water to reach its current density.

ACKNOWLEDGMENTS

We acknowledge helpful discussion with Robert Millis, John Spencer, Jim Elliot, and Leslie Young. Marc Buie and Elliot Young were kind enough to supply their albedo maps in digital form for our use in this project and also participated in useful discussions. The Toowoomba data greatly improved our ability to convincingly demonstrate the similarity between our model lightcurves and the occultation data, and were kindly provided by Larry Wasserman and Robert Millis. This work was supported by NASA Grant NAGW-1039.

REFERENCES

ALTENHOFF, W. J., R. CHINI, H. HEIN, E. KREYSA, P. G. MEZGER, C. SALTER, AND J. B. SCHRAML 1988. First radio astronomical estimate of the temperature of Pluto. *Astron. Astrophys.* **190,** L15–17.

ANDERS, E., AND M. EBIHARA 1982. Solar system abundances of the elements. *Geochim. Cosmochim. Acta* **46,** 2363–2380.

ANDERS, E., AND N. GREVESSE 1989. Abundances of the elements: Meteoritic and solar. *Geochim. Cosmochim. Acta* **53,** 197–214.

BATES D. R. 1951. The temperature of the upper atmosphere. *Proc. Phys. Soc. B* **64,** 805–821.

BUIE, M. W., D. J. THOLEN, AND K. HORNE 1992. Albedo maps of Pluto and Charon: Initial mutual event results. *Icarus* **97,** 211–227.

ELLIOT, J. L., E. W. DUNHAM, A. S. BOSH, S. M. SLIVAN, L. A. YOUNG, L. H. WASSERMAN, AND R. L. MILLIS 1989. Pluto's atmosphere. *Icarus* **77,** 148–170.

ELLIOT, J. L., AND L. A. YOUNG 1992. Analysis of stellar occultation data for planetary atmospheres. I. Model fitting, with application to Pluto. *Astron. J.* **103,** 991–1015.

ENGEL, S., J. I. LUNINE, AND J. S. LEWIS 1990. Solar nebula origin for volatile gases in Halley's comet. *Icarus* **85,** 380–393.

ESHLEMAN, V. R. 1989. Pluto's atmosphere: Models based on refraction, inversion and vapor-pressure equilibrium. *Icarus* **80,** 439–443.

GREVESSE, N., D. L. LAMBERT, A. J. SAUVAL., E. F. VAN DISHOECK, C. B. FARMER, AND R. H. NORTON 1991. Vibration–rotation bands of CH in the solar infrared spectrum and the solar carbon abundance. *Astron. Astrophys.* **242,** 488–495.

HAPKE, B. 1981. Bidirectional reflectance spectroscopy. I. Theory. *J. Geophys. Res.* **86,** 3039–3054.

HIRSCHFELDER, J. O., C. F. CURTISS, AND R. B. BIRD 1964. *Molecular Theory of Gases and Liquids.* Wiley, New York.

HUBBARD, W. B., D. M. HUNTEN, S. W. DIETERS, K. M. HILL, AND R. D.WATSON 1989. Occultation evidence for an atmosphere on Pluto. *Nature* **336,** 452–454.

HUBBARD, W. B., R. V. YELLE, AND J. I. LUNINE 1990. Nonisothermal Pluto atmosphere models. *Icarus* **84,** 1–11.

JEWITT, D. C. 1994. Heat from Pluto. *Astron. J.* **107,** 372–378.

LEWIS, J. S., AND R. G. PRINN 1980. Kinetic inhibition of CO and N_2 reduction in the solar nebula. *Astrophys. J.* **238,** 357–364.

LUNINE, J. I., S. ENGEL, B. RIZK, AND M. HORANYI 1991. Sublimation and reformation of icy grains in the primitive solar nebula. *Icarus* **94,** 333–344.

MCKINNON, W. B. 1989. Impact jetting of water ice with application to the accretion of icy planetesimals and Pluto. *Geophys. Res. Lett.* **16,** 1237–1240.

MCKINNON, W. B., AND S. MUELLER 1988. Pluto's structure and composition suggest origin in the solar and not a planetary nebula. *Nature* **335,** 240–243.

MILLIS, R. L., L. H. WASSERMAN, O. G. FRANZ, R. A. NYE, J. L. ELLIOT, E. W. DUNHAM, A. S. BOSH, L. A. YOUNG, S. M. SLIVAN, A. C. GILMORE, P. M. KILMARTIN, W. H. ALLEN, R. D. WATSON, S. W. DIETERS, K. M. HILL, A. B. GILES, G. BLOW, J. PRIESTLY, W. M. KISSLING, W. S. G., WALKER, B. F. MARINO, D. G. DIX, A. PAGE, J. E. ROSS, H. D. KENNEDY, AND A. R. KLEMOLA 1994. Pluto's radius and atmosphere: Results from the entire 9 June 1988 occultation data set. *Icarus* **105,** 282–297.

NARAYAN, R., AND W. B. HUBBARD 1988. Theory of anisotropic refractive scintillation: Application to stellar occultations by Neptune. *Astrophys. J.* **325,** 503–518.

NULL, G. W., W. M. OWEN, JR., AND S. P. SYNNOTT 1993. Masses and densities of Pluto and Charon. *Astron. J.* **105,** 2319–2335.

OWEN, T. C., T. L. ROUSH, D. P. CRUIKSHANK, J. L. ELLIOT, L. A. YOUNG, C. DEBERGH, B. SCHMITT, T. R. GEBALL, R. H. BROWN, AND M. J. BARTHOLOMEW 1993. Surface ices and the atmospheric composition of Pluto. *Science* **261,** 745–748.

RAGES, K., AND J. B. POLLACK 1992. Voyager imaging of Triton's clouds and hazes. *Icarus* **99,** 289–301.

SIMONELLI, D. P., AND R. T. REYNOLDS 1989. The interiors of Pluto and Charon: Structure, composition and implications. *Geophys. Res. Lett.* **16,** 1209–1212.

STANSBERRY, J. A., R. V. YELLE, J. I. LUNINE, AND A. S. MCEWEN 1992. Energy coupling between Triton's surface and atmosphere. *Icarus* **99,** 242–260.

STERN, S. A. 1992. The pluto–Charon system. *Annu. Rev. Astron. Astrophys.* **30,** 185–233.

STERN, S. A., D. A. WEINTRAUB, AND M. C. FESTOU 1993. Evidence for a low surface temperature on Pluto from millimeter-wave thermal emission measurements. *Science* **261,** 1713–1716.

STEVENSON, D. J. 1990. Chemical heterogeneity and imperfect mixing in the solar nebula. *Astrophys. J.* **348,** 730–737.

SYKES, M. V., R. M. CUTRI, L. A. LEBOFSKY, AND R. P. BINZEL 1987. IRAS serendipitous observations of Pluto and Charon. *Science* **237,** 1376–1340.

TYLER, G. L., D. N. SWETNAM, J. D. ANDERSON, S. E. BORUTZKI, J. K. CAMPBELL, E. R. KURSINSKI, G. S. LEVY, G. R. LINDAL, J. R. LYONS, E. A. MAROUF, P. A. ROSEN, R. A. SIMPSON, AND G. E. WOOD 1989. Voyager radio science observations of Neptune and Triton. *Science* **246,** 1466–1473.

VAN DISHOECK, E. F., G. A. BLAKE, B. T. DRAINE, AND J. I. LUNINE 1993. The chemical evolution of protostellar and protoplanetary matter. In *Protostars and Planets III* (E. H. Levy and J. I. Lunine, Eds.), pp. 163–241. Univ. of Arizona Press, Tucson.

YELLE, R. V., AND J. I. LUNINE 1989. Evidence for a molecule heavier than methane in the atmosphere of Pluto. *Nature* **399,** 288–290.

YELLE, R. V., J. I. LUNINE, AND D. M. HUNTEN 1991. Energy balance and plume dynamics in Triton's lower atmosphere. *Icarus* **89,** 347–358.

YOUNG, E. F., AND R. P. BINZEL 1993. Comparative mapping of Pluto's sub-Charon hemisphere: Three least squares models based on mutual event lightcurves. *Icarus* **102,** 134–149.

YOUNG, L. A., C. B. OLKIN, J. L. ELLIOT, D. J. THOLEN, AND M. W. BUIE 1994. The Charon–Pluto mass ratio from MKO astrometry. *Icarus,* **108,** 186–199.